4230 *Macromolecules* **2009**, *42*, 4230–4236
DOI: 10.1021/ma900382t

Macromolecules
ARTICLE

Determination of the Ordered Structure in Conjugated-Coil Diblock Copolymers Films from a Thickness Gradient Prepared by Spin-Coated Drop Technique

M. Al-Hussein,*,† M. A. Ruderer,‡ E. Metwalli,‡ V. Körstgens,‡ U. Vainio,§ S. V. Roth,§ R. Döhrmann,§ R. Gehrke,§ R. Gebhardt,⊥ M. Burghammer,⊥ and P. Müller-Buschbaum‡

†*Department of Physics, University of Jordan, Amman 11942, Jordan,* ‡*TU München, Physik-Department, LS E13, James-Franck-Str.1, 85747 Garching, Germany,* §*HASYLAB at DESY, Notkestr. 85, 22603 Hamburg, Germany, and* ⊥*ESRF, BP 220, F-38043, Grenoble Cedex 09, France*

Received February 19, 2009; Revised Manuscript Received May 3, 2009

ABSTRACT: Investigating the thickness dependence of ordered structure of thin films of electrically conducting conjugated polymers with nano-ordered morphologies is essential for optimizing their applications in advanced electrooptic devices. We demonstrate here that by spin-coating a small drop of a conjugated-coil diblock copolymer, a thickness gradient varying between tens of nanometers to a few micrometers is formed at the drop rim. Compared to other widely used solution casting methods for the preparation of thickness gradients, the spin-coated drop technique produces film gradients with thickness in the interesting range for most applications in an extremely short preparation time. Using a submicrometer-sized X-ray beam and a scanning technique, spatial mappings of the gradient area are obtained with submicrometer grazing incidence small-angle X-ray scattering (sub-μGISAXS) for the first time. Investigating the thickness gradient with sub-μGISAXS has the advantage of saving the preparations and investigations of many samples each with a certain thickness under identical conditions. As a model system, we use the diblock copolymer polystyrene-*block*-poly(*p*-phenylene) with a thickness gradient ranging between 80 and 2280 nm. Detailed analysis of the scattering patterns at selected positions along the gradient identifies a regime of lateral order within a thickness range of 80−210 nm.

1. Introduction

Electrically conducting conjugated polymers are attracting much interest due to their potential applications in new electrooptic devices such as inexpensive and flexible LEDs, transistors, and photovoltaic cells.[1−5] Producing phase-separated structures of these polymers with controlled size and shape on the nanoscale constitutes a promising approach in the fields of organic photovoltaics and molecular electronics.[6−13] One nonlithographic approach to achieve such nanostructures is offered by the synthesis of block copolymers including at least one conjugated sequence. Block copolymers have the ability to self-assemble into a series of periodic microdomains with a 10−100 nm period through microphase separation in the solid state or micellization in solution.[14−23] Their morphology can be adjusted by changing the chemical structures of the constituting blocks as well as their conformational properties and composition. The various morphologies resulting from the microphase separation have been described in detail for copolymers in which the components are made of flexible chains (coil−coil copolymers).[14] However, the incorporation of a rodlike conjugated sequence into a block copolymer results in a rod−coil molecular structure and significant changes in the observed morphologies compared to coil−coil copolymers.[24,25] This is because the self-assembly of rod−coil copolymers is no longer solely determined by the microphase separation of its constituent blocks but is also affected by the liquid crystalline or crystalline ordering of the rod block.[26−32]

The optical, electrical, and mechanical properties of thin solid films of conjugated-coil copolymers intimately depend on the intermolecular interactions, and these in turn are dependent on the packing of the copolymer molecules. Therefore, the controlled preparation of thin films of well-ordered nanometer-sized structures with chemical functionalities and physical properties of conjugated polymers opens the possibility of controlling optoelectronic properties such as light emission, charge transfer, and charge transport on the nanoscale. Well-ordered thin films of conjugated polymers have been prepared using various techniques (e.g., solution casting, pulsed laser deposition, Langmuir−Blodgett, spin-coating).[4,33]The spin-coating technique has emerged as a popular choice because of the advantages it offers compared to the other techniques; it is fast and less demanding. Moreover, spin-coating is widely used in industry and thus promising for applications.

A detailed investigation of the film morphology and understanding the ordering of conjugated-coil block copolymers in thin films, where geometric confinement and surface segregation play a large role in determining the microphase structure, is essential for optimizing the properties of conjugated materials. To this end, several techniques have been used. Among these techniques, grazing incidence small-angle X-ray scattering (GISAXS) has proven to be a powerful advanced scattering technique for the investigation of nanostructured films. Its potential as a nondestructive technique for determining depth-dependent information regarding the nanostructure and morphology of patterned thin nanocomposites and polymer films has been widely exploited.[34−42] Employing a submicrofocus X-ray beam with a reflection geometry, a submicrofocus grazing-incidence small-angle X-ray scattering (sub-μGISAXS) is realized, opening up new possibilities.[39] The small beam size reduces the illuminated

*Corresponding author. E-mail: m.alhussein@ju.edu.jo.

 Published on Web 05/19/2009

sample volume and thus offers the opportunity to achieve position-sensitive scattering information even on locally curved surfaces.[42] Together with a scanning technique, spatial mappings of inhomogeneous thin films become possible.[41−43]

Here, we first demonstrate that a drop with a thickness gradient of a conjugate-coil diblock copolymer can be prepared by the spin-coating technique. Then, by scanning the gradient with a sub-μ-focus X-ray beam, we are able to investigate the structure and morphology of different positions along the gradient. This combinatorial approach is equivalent to investigating many single films of different thicknesses prepared under exactly the same conditions, thus saving the preparations and investigations of many samples each having a certain thickness.[44] The model system we used in this study is a diblock copolymer containing a fully conjugated poly(*p*-phenylene) (PPP) segment, associated with a polystyrene (PS) block, P(S-*b*-PP). Dynamic light scattering results show that the diblock forms micellar objects in toluene solution. These micelles constitute the basic units in spin-coated thin films after solvent evaporation too. AFM images show that they are spherical in shape regardless of the film thickness. Detailed sub-μGISAXS measurements reveal thickness-dependent lateral ordering of these micelles. For thicknesses up to 210 nm, the micelles are packed in monolayers with the layers normals oriented parallel to the film surface and an interlayer period of about 19 nm.

2. Experimental Section

2.1. Samples. The diblock copolymer investigated was purchased from Polymer Source, Inc., and used as received. It consists of poly(styrene) and poly(*p*-phenylene) blocks (P(S-*b*-PP)) with M_n of the PS and PPP blocks of 5700 and 2900, respectively. This results in about 0.23 volume fraction of the PPP block. The polydispersity (M_w/M_n) of the diblock copolymer is 1.14.

2.1.1. Solution Preparation. Solutions with concentrations ranging from 0.5 to 25 mg/mL were prepared by dissolving the copolymer powder in a filtered toluene solution at ambient conditions. The solution was stirred for about 2 h and then filtered with a 0.2 μm PTFE filter. A clear colored (dark red) solution was obtained.

2.1.2. Film Preparation. The gradient was prepared by spin-coating a 30 μL drop of 25 mg/mL toluene solution onto a silicon substrate at 3000 rpm for 30 s. The silicon substrate was cleaned prior to spin-coating with hydrofuran (HF) solution to start with a defined chemical surface. For the spin-coated drop technique it is essential that the amount of the solution did not cover the whole substrate area so that the solution would not reach the substrate edge during the spinning process. No subsequent annealing was performed on the resulting film. This resulted in a somewhat circular thin film with a homogeneous thickness in the central region and a thickness gradient at the rim.

2.2. Dynamic Light Scattering (DLS). Possible association of the P(S-*b*-PP) diblock in solution was studied by dynamic light scattering (DLS) using a dynamic light scattering spectrometer with goniometer and monomode fiber detection (ALV-Laser GmbH, Langen). The laser used was a 150 mW frequency-doubled Nd:YAG laser at 532 nm (Coherent DPSS 532-150). Polymer solutions were filtered directly into dust-free light scattering cells. The correlation function of the scattered intensity was calculated using an ALV-5000 correlator on a logarithmic time scale ranging from 10 ns to 10 s. Data of transparent solutions were collected at scattering angles of 90°. The temperature was controlled by a thermostat bath and was set at 20 °C. The hydrodynamic diameter (D_h) and the size distribution of the aggregates were obtained by analyzing the experimental intensity correlation function as described elsewhere.[45]

2.3. Optical Investigation. The film surface was observed with optical microscopy using a Zeiss Axiotech 25H optical microscope. A Hitachi KP-D50 CCD camera recorded the micrographs with a magnification ranging between 1.25 and 100.

2.4. Atomic Force Microscopy. The surface morphology of the thin film was investigated by atomic force microscopy (AFM) at room temperature using a PARK Autoprobe CP atomic force microscope. Imaging was done in the noncontact mode using standard silicon cantilevers with a resonant frequency of about 80 kHz and a silicon tip with a curvature radius of 10 nm and a spring constant of 2.1 N/m. AFM topographic images were used also to determine the thickness profile of the drop after making a scratch across the drop.

2.5. Submicrobeam Grazing Incidence Small-Angle X-ray Scattering (Sub-μGISAXS). Sub-μGISAXS experiments were conducted at the ID13 Beamline (ESRF, Grenoble) at a wavelength of $\lambda = 0.097$ nm. The beam was focused to the size of $(0.5 \times 1.0)\ \mu m^2$ using an assembly of Fresnel zone plates. For the basic setup, see ref 39. The sample was placed horizontally (xy plane), and the X-ray beam impinged on the sample under a fixed incident angle of $\alpha_i = 0.62°$ (see Figure 1). The resulting footprint on the sample was $0.5 \times 92.4\ \mu m^2$. The thickness gradient was placed perpendicular to the X-ray beam direction and scanned at different y positions using a step size of 10 μm by shifting the sample in the submicrobeam along the gradient. The scattering patterns were recorded with a 2D MAR-CCD detector with a pixel size of 79 μm at a distance of 840 mm from the sample. Radiation damage was avoided by properly adjusting the exposure time between 1 and 100 s. The primary beam and the strong specular reflection from the sample were blocked by lead beam stops to avoid saturation of the detector.[35] The resulting data set was a map of intensity $I(\Psi,\alpha_f)$, where Ψ is the out-of-plane angle and α_f is the exit angle. The chosen incident angle is well above the critical angle of both the polymer film and the substrate (α_c(P(S-*b*-PP)) = 0.102°, α_c(Si) = 0.144°); therefore, the Yoneda peaks of both polymer blocks and the specular peak are well separated on the 2D detector. Moreover, at this angle of incidence ($\alpha_i > \alpha_c$) surface and bulk nanostructures of the polymer film are accessible. Scattering angles were converted into q-space. Structural information is obtained then using line cuts: horizontal cuts (q_y cuts) at constant q_z value and vertical cuts (q_z cuts) at constant q_y value of the 2D intensity distribution with $q_y = 2\pi/\lambda(\sin\Psi\cos\alpha_f)$ and $q_z = 2\pi/\lambda[\sin\alpha_i + \sin\alpha_f]$.[35,38] While the horizontal cuts are used to obtain information about the lateral structure, the vertical cuts provide information about the structure normal to the sample surface. Generally, the vertical cuts are presented as plots of the scattering intensity versus the detector angle, $\Phi = \alpha_i + \alpha_f$. To improve statistics, all cuts were integrated over a limited q-range.

3. Results

3.1. Solution Aggregation. The association of the P(S-*b*-PP) copolymer in toluene solution was probed by DLS first. Figure 2 shows a typical intensity−intensity correlation function for a solution with a 25 mg/mL concentration. The correlation function was then analyzed to deduce the size distribution function.[45] Two different populations are observed: the first one is nearly monodisperse with D_h at 20 nm, and the second one is more polydisperse with D_h at 65 nm. Similar general behavior has been exhibited by all solutions regardless of their concentrations. This clearly shows that although toluene is nominally a good solvent for both blocks aggregates of the P(S-*b*-PP) copolymer are formed in solution. Information regarding the shape of these aggregates was provided by AFM images of thin films prepared from these solutions as shown below.

3.2. Thin Films. A thickness gradient of the P(S-*b*-PP) copolymer was prepared with the spin-coating drop technique as described above. No additional solvent or thermal annealing was carried out in order to trap the aggregates

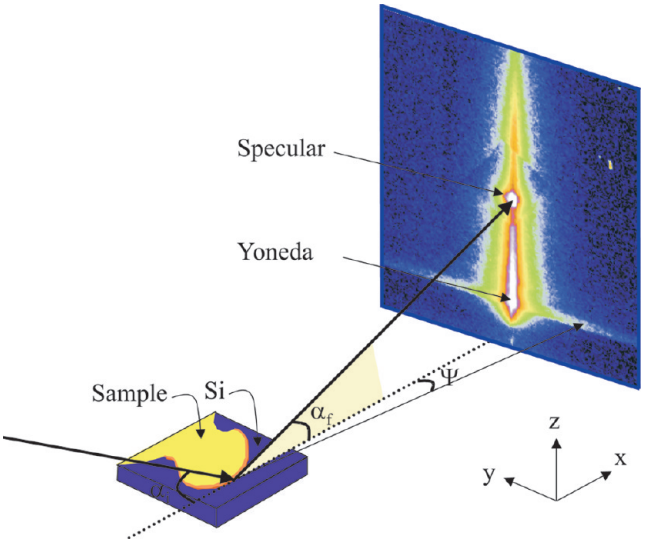

Figure 1. Schematic drawing of the μGISAXS experimental setup. The sample is placed horizontally (xy plane), and the X-ray beam impinged on the sample under a fixed incident angle of $\alpha_i = 0.62°$. The thickness gradient is placed perpendicular to the beam and scanned at different y positions using a step size of 10 μm by shifting the sample in the microbeam along the y-direction across the gradient.

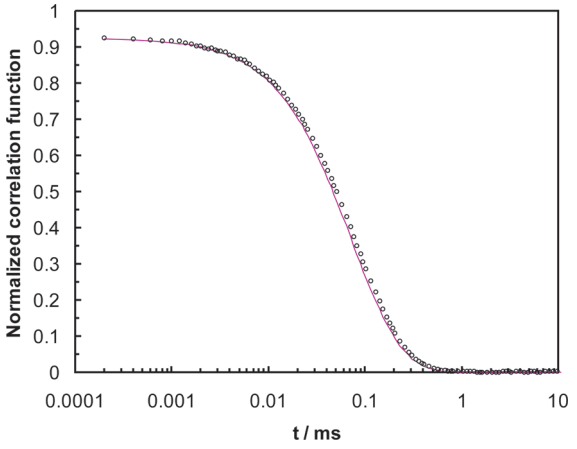

Figure 2. A typical measured (circles) intensity−intensity correlation function for a solution with a 9 mg/mL concentration. The solid line is the best fit calculated from the radial size distribution, as measured with DLS.

formed in solution and not to modify them. Figure 3 shows an optical image of the resulting film. As can be seen, while the central part of the drop exhibits only one color due to its homogeneous thickness, different interference colors are exhibited at the rim of the drop indicating a varying thickness of the film in this region. As it is difficult to extract height information from this optical image, we tried other methods. Attempts to quantify the thickness gradient using imaging ellipsometry with a spatial resolution of 2 μm were not successful due to the difficult nature of the gradient.[35] Therefore, we resorted to a more destructive method. First, a scratch along the gradient was made carefully using a sharp needle. It was made sure that the scratch did not affect the silicon substrate underneath the film. Then the depth of this scratch was constructed from height profiles of successive AFM images along it. The resulting thickness profile is shown in Figure 4; the thickness is denoted by t, while the distance from the rim is denoted by d. The drop exhibits a thick outer ring (height ~ 2200 nm), then the thickness drops to around 80 nm, next it increases gradually to about 400 nm,

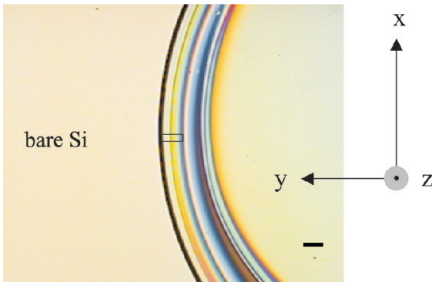

Figure 3. Optical microscope image of a spin-coated drop. The scanned area is marked by the black rectangle. The bar size is 300 μm.

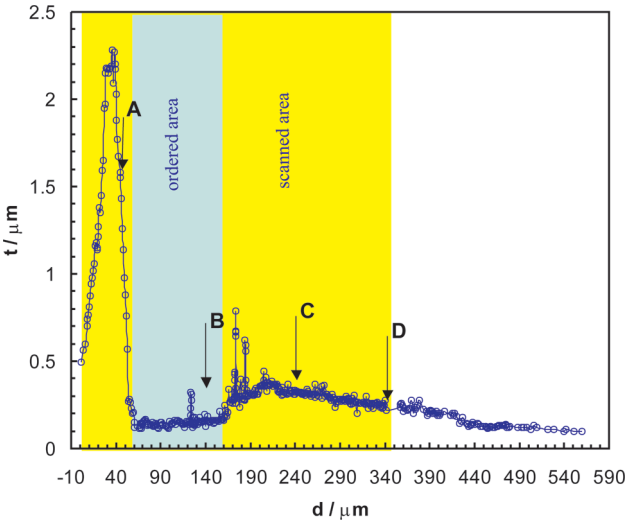

Figure 4. Thickness profile for the spin-coated drop as deduced from successive topographic AFM images taken along a scratch made through the thickness gradient. Position A is at thickness of 1500, position B lies at 100 μm from position A inside the drop at thickness of 185 nm, position C is at 100 μm from position B at thickness of 320 nm, and position D is at 100 μm from position C at thickness 250 nm.

and finally it decreases again until it reaches the homogeneous central part of the film of thickness around 80 nm. This shows that a drop with a thickness gradient ranging between 80 and 2200 nm is accessible using spin-coating. The gradient area can be considered as an ensemble of many spin-coated films each with a specific thickness. One can vary the range of the gradient using other solution concentrations. Nonetheless, the maximum thickness achieved, ~2200 nm, is large enough for most applications. On the other hand, very thin films cause dewetting, and thus the rim will be detached from the central part of the drop. Therefore, a concentration of 25 mg/mL seems a good choice for the P(S-*b*-PP) copolymer. The morphology at selected places of different thicknesses of the drop was investigated by AFM. Figure 5 shows representing topographic images at four different positions along the thickness gradient. Position A has a thickness of 1500 nm, position B lies at 100 μm from position A inside the drop with a thickness of 185 nm, position C is at 100 μm from position B with a thickness of 320 nm, and position D is at 100 μm from position C with a thickness 250 nm (see Figure 4). All images show somewhat spherical objects with different sizes and some depressions on the surfaces of 3−5 nm depth. Evidently, the appearance of the spherical objects is independent of the film thickness. However, AFM can only probe the surface with no insights regarding the inner structure of the film. With scattering methods such structures become accessible. GISAXS has been the technique of choice in thin film geometries. In conventional

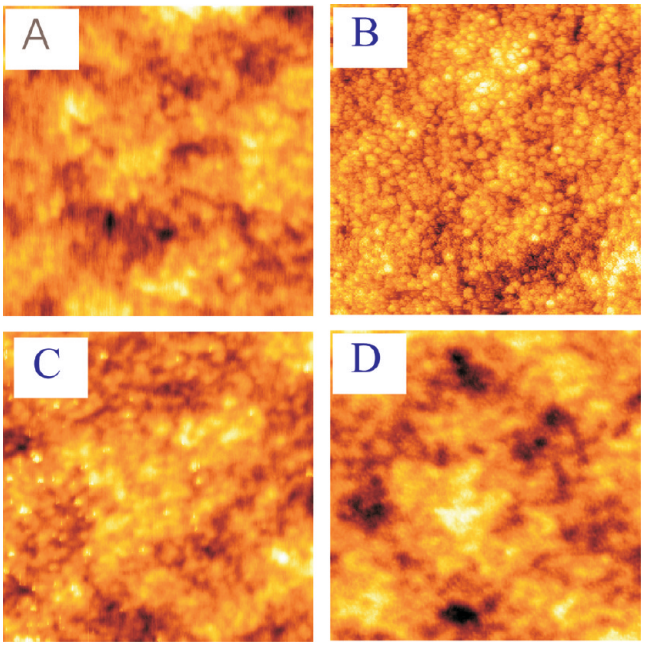

Figure 5. Representative AFM topographic images at position A, B, C, and D of Figure 4. The size of each image is $2 \times 2\ \mu m^2$. For clarity of representation, the color bar is adjusted for each image independently.

GISAXS, the X-ray beam has typically a diameter of 400 μm, which renders it unsuitable for our drop. Because of the large size of the beam compared to the gradient area, the scattering signal would be averaged over most of the gradient area and thus losing local structural information. Moreover, because of the curvature of the drop, scattering with a beam of a comparable size to the curvature radius would give a distorted GISAXS signal. A typical μ-focus beam has a diameter of 5 μm, which is still big for probing our drop. To overcome these problems, we used a sub-μ-focus beam to perform GISAXS. An X-ray beam with a diameter of only 0.5 μm is used; thus, local ordered structures parallel and perpendicular to the surface throughout the whole film became attainable. Sub-μGISAXS patterns were recorded at 35 positions along the gradient, starting at the drop rim and scanning toward the center of the drop with a step size of 10 μm. Because of the small beam size, each pattern represents a film of a certain thickness and has to be treated separately. Figure 6 presents representative patterns at positions A, B, C, and D defined above. Common features of the patterns are the specular peak and the diffuse scattering including the Yoneda peak. Although the AFM images shown in Figure 5 look basically similar, their corresponding scattering patterns show some differences in the region of the Yoneda peak. In pattern A, only a weak Yoneda peak is observed with no pronounced out-of-plane scattering. In pattern B, strong two streaks are visible, which can be taken as a sign of order. In pattern C, the two streaks merge into a diffuse less pronounced streak. Finally in pattern D, the single streak becomes smaller and weaker in intensity. To obtain more quantitative data, we performed horizontal and vertical line cuts for each pattern. As for the horizontal cuts, we performed them at a fixed exit angle corresponding to the Yoneda peak of the copolymer. Figure 7 shows the intensity distribution as a function of q_y, along the out-of plane direction at the four positions of Figure 4. A broad peak at $q_y = 0.33\ nm^{-1}$ can be seen more pronounced in some patterns than others. The solid line is the best fit of the whole curve obtained using two Lorentzians plus a constant background. The results of all fits performed on the 35 patterns

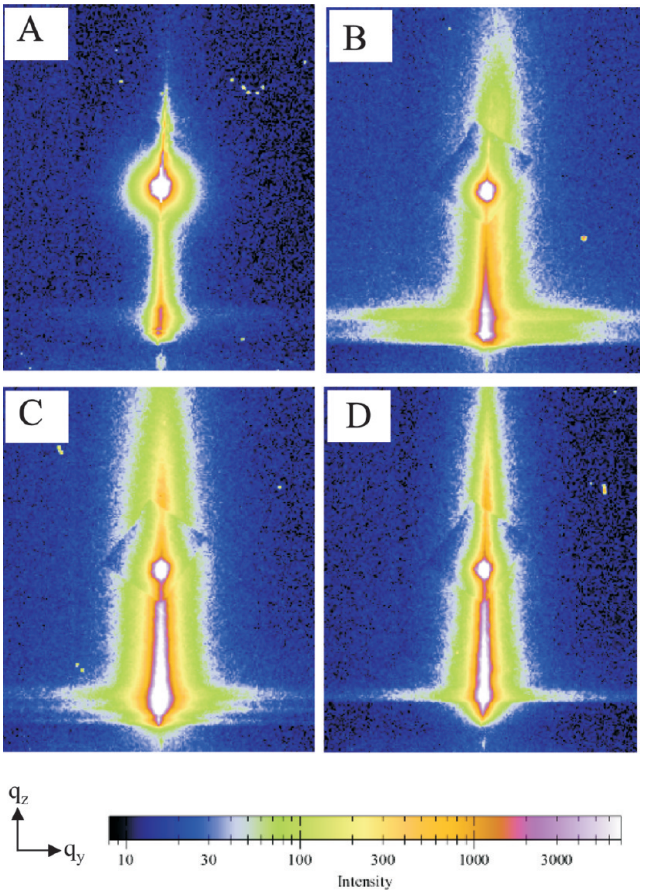

Figure 6. Sub-μGISAXS patterns obtained at position A, B, C, and D of Figure 4. In each pattern q_y varies between -0.717 and $0.700\ nm^{-1}$ and q_z varies between 0.545 and $2.20\ nm^{-1}$.

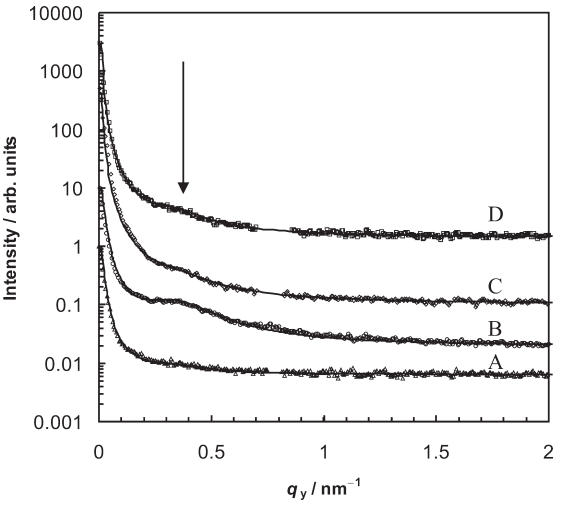

Figure 7. Intensity distribution as a function of q_y, along the out-of plane direction at the four positions of Figure 4. The curves are shifted along the y-axis for clarity. The solid line is the best fit of the whole curve obtained using two Lorentzians plus a constant background.

are summarized by plotting the normalized intensity and the full width at half-maximum (fwhm) of this peak as functions of the scanned position in Figure 8. The distance from the rim can be translated into film thickness using Figure 4. The curve shows a peak in intensity and a minimum in the fwhm in the range of 60−170 μm distance from the rim. To investigate any possible layering along the normal to the film surface, we performed q_z line cuts. Such layering is

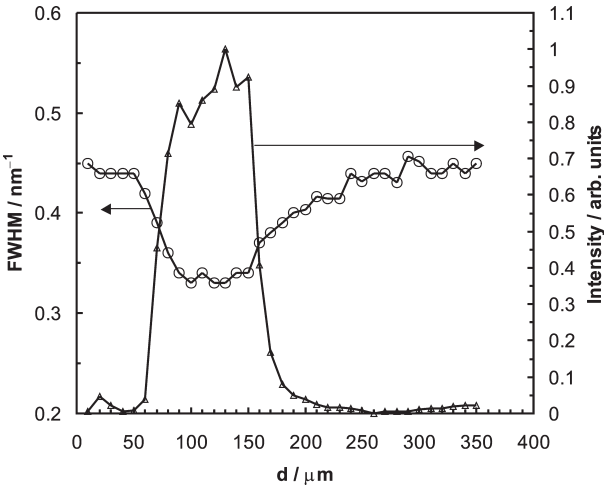

Figure 8. Intensity of the peak at $q_y = 0.33$ nm^{-1} normalized to film thickness as a function of the distance from the rim for the 35 patterns.

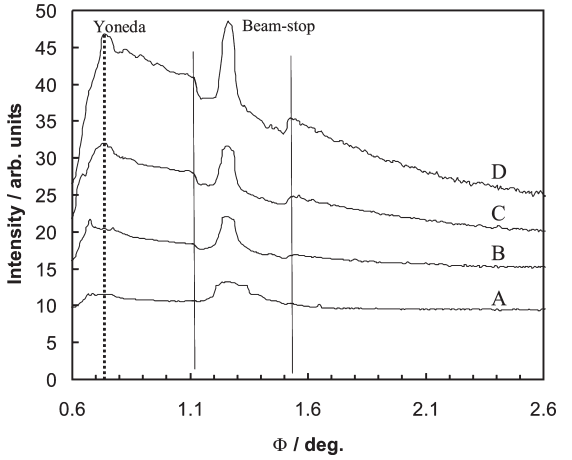

Figure 9. Intensity distribution as a function of q_z, along the normal to the direction at the four positions of Figure 4. The curves are shifted along the y-axis for clarity.

evidenced by the appearance of Bragg peaks in the curve of the scattering intensity versus the detector angle corresponding to the periodic spacing. Figure 9 shows representative curves at positions A, B, C, and D in a semilog scale. Obviously, none of the curves show any discernible Bragg peaks.

4. Discussion

The DLS results presented confirm the formation of micellar objects in the solution of the P(S-*b*-PP) copolymer. This might come as a surprise since toluene is a good solvent for both blocks, and therefore the formation of aggregates in the solution is not expected. The size distribution of these aggregates shows a bimodal distribution with peaks at sizes of about 20 and 65 nm. Information about their shape cannot be deduced from our DLS. Therefore, we turned to the AFM results of thin films prepared from these solutions by spin-coating. To ensure that the morphology observed in the thin film is mostly from the preformed aggregations in solution, no annealing was performed subsequent to the spin-coating. The AFM topographic images of Figure 5 clearly show that the aggregates have somewhat a spherical shape. They bear striking similarities with thin films of spherical casein micelles.[45,46] The 3−5 nm depressions may be attributed to the irregular packing of these spherical objects along the film thickness. The question that arises now is, what is

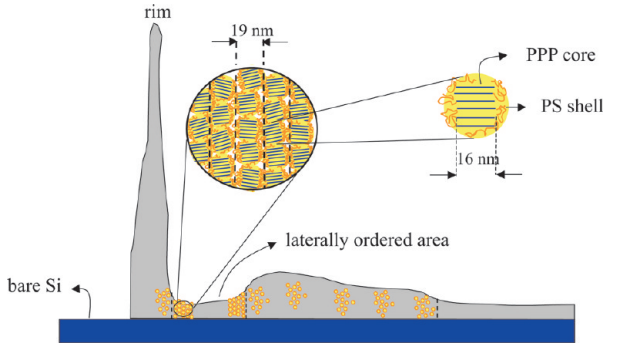

Figure 10. Schematic drawing for a possible model of the spin-coated drop structure of the P(S-*b*-PP) diblock copolymer.

responsible for the formation of these spherical micelles? According to the phase diagram of a coil−coil diblock copolymers, cylinders of PPP (the minor block) in a matrix of PS (the major block) are the expected morphology and not spheres (the volume fraction of the PPP block is about 0.23).[14] Moreover, the possibility of micellization of one of the blocks due to a selective solubility is ruled out since toluene is a good solvent for both blocks of the P(S-*b*-PP) copolymer. However, the conjugated chains of the PPP block have a strong tendency to self-organize in liquid crystalline or crystalline structures due to their rodlike nature. This in turn can provide the necessary driving force for the copolymer to form aggregates in solution. We attribute the smaller size object (20 nm) to a single spherical micellar object, whereas the larger one can be attributed to a loose aggregates of these small micelles as have been seen for many micellar copolymer solutions.[47] Each micelle is made of a dense PPP core surrounded by a PS shell (Figure 10). The PS chains are fully dissolved and therefore fan out of the PPP core, giving the micelle its somewhat spherical shape. The molecular weight of the PPP block (2900) corresponds to an average of 38 phenylene units per chain. Consequently, the extended length of the PPP chain is about 16 nm, estimated using the degree of polymerization and the known repeating unit length projected to the chain axis of PPP (~0.43 nm).[48] Furthermore, the PPP segment is very rigid and does not fold. This suggests an interdigidated packing of the PPP chains with only one chain across the PPP core of the micelle. In each core, the PPP molecules can organize in either a head-to-head (nonconjugated blocks lie on the same side of the conjugated blocks) or head-to-tail configuration (adjacent nonconjugated blocks lie on opposite sides of the conjugated blocks). However, molecular dynamic calculations showed that the latter case is more energetically favorable as it allows for considerable coiling of the nonconjugated blocks while maintaining the conjugated block in regular dense assemblies.[48]

So far spin-coating has been used to produce uniform films of polymers but not films with thickness gradient. Common spin-coating without introducing gradients is already a complex process; nevertheless, it can be simplified using a three-step model. First, the polymer solution is dispensed onto the center of a stationary substrate, and then the substrate starts spinning at a high speed (typically around 3000 rpm). An excessive amount of solution is usually used to ensure a full coverage of the substrate which will lead to a continuous film. During this step, the centripetal acceleration causes the solution to spread to and eventually off the edge of the substrate, leaving a thin film of the solution on the surface. The second step involves further thinning of the solution layer deposited until enough solvent has been removed by evaporation. In the third step, evaporation of the solvent dominates the process, and a solid homogeneous thin polymer film is obtained. In the spin-coated drop technique, the basic modification to common spin-coating is the use of only

a small solution material to ensure that the solution will not reach the substrate edge during spinning. In this case, the radial flow of material during the thinning of the central part of the drop causes the accumulation of more material at the drop rim as it cannot reach the substrate edge. Meanwhile, fast evaporation of the solvent takes place in the rim area, the triple phase boundary line,[42] leading to more loss of the solvent there. This gives rise to a gradient in the solvent concentration, to compensate this loss more flow of material toward the rim takes place. The continuous evaporation of the solvent gradually increases the viscosity to a level where flow ceases. This effectively leads to different parts of the film in the rim area have different thicknesses. Therefore, with the modified approach spin-coating can be used to prepare drop samples with thickness gradient.

Although the AFM data of the surface morphology show spherical aggregates at all thicknesses of the drop, detailed sub-μGISAXS revealed subtle differences in the lateral ordering of the micellar objects at different positions along the gradient. The horizontal cuts of the 35 patterns show a relatively broad peak at $q_y = 0.33\ \mathrm{nm}^{-1}$, indicating a lateral ordering. The appearance of this peak varies between the patterns. It is very discernible in some patterns but hardly seen in others. This clearly indicates a varying in-plane ordering of the micellar objects throughout the film. The corresponding periodic spacing of this peak is ~19 nm. This comes very close to the size seen by DLS of a single micellar object, suggesting that these micellar objects are closely packed laterally for certain positions along the gradient. A plot of the intensity and the fwhm of the peak as functions of the distance from the rim inward shows clearly a peak in intensity and a minimum in the fwhm at a distance 60−170 μm from the rim. In terms of film thickness, this shows that the lateral packing of these micellar objects is the best for film thickness less than 210 nm. Such information is very useful in the field of conjugated polymeric films. For instance, in photovoltaic cells applications it is important to prepare the thickest film possible with a desired structure in order to achieve maximum light harvesting. Finally, a careful inspection of the vertical cuts, including the area of the beam-stop shadow, shows no evidence for a layering of these micellar objects normal to the substrate in the observed q-range. This suggests that the micelles merge together inside each layer with the PS blocks acting as glue between the PPP cores. However, we do observe a diffraction arc in the wide-angle q-range reflecting the π-stacking of the PPP chains. On the basis of these observations and the arguments used above, we can propose a model of the drop structure as shown in Figure 10. The PPP blocks tend to form stable π-stacks while the PS blocks tend to coil. Their confinement in thin films promotes their packing in monolayers parallel to the film surface. This is best seen for films thinner than 210 nm. For thicker films, however, the lateral order diminishes due to less confinement. It should be mentioned here that because the drop was not annealed, the lateral ordering cannot be attributed to the film thickness solely. For example, one can think of a solvent transport-dependent process that leads to kinetically trapped morphologies.[49] Moreover, other more elaborate methods can be used to prepare films with a smoother gradient. Nonetheless, the main objectives of our work are first to demonstrate that the well-known edge effect in spun-cast films, which is widely considered as a "nuisance" by most researchers, can be used to prepare thickness gradients in a fast less demanding way. Second, with a submicro-GISAXS, one can quantify the nano-order and molecular packing at different thicknesses for such a difficult gradient of the drop sample.

This approach of preparing a spin-coated drop with a thickness gradient at its rim works not only for conjugated-coil diblock copolymers, but we found that it works for polymer blend systems, too. Furthermore, it is likely that other conjugated diblock copolymers form aggregations in good solvent of the coil block, and this can be used to fabricate thin films with desirable but nonequilibrium morphologies in many devices.

5. Conclusions

Sub-μGISAXS performed on a thin film with thickness gradient can reveal detailed thickness-dependent information regarding the morphology and molecular packing of thin films of conjugated-coil block copolymers. Such a film can be prepared by spin-coating a small drop of the copolymer solution. This has been demonstrated using a diblock copolymer containing a fully conjugated poly(*p*-phenylene) (PPP) segment, associated with a polystyrene (PS) block, P(S-*b*-PP). Dynamic light scattering results show that the diblock forms micellar objects in toluene solution. These micelles were trapped in spin-coated thin films after solvent evaporation. AFM images show that they are spherical in shape regardless of the film thickness. Detailed sub-μGISAXS reveal thickness-dependent lateral ordering of these micelles. For thicknesses up to 210 nm, the micelles are packed in monolayers with the layer normals oriented parallel to the film surface and a period of 19 nm.

Acknowledgment. M.A.H. acknowledges the financial support by the IAEA fellowship within the framework of the capacity building program of SESAME. M.A.R. acknowledges the Bavarian State Ministry of Science, Research and Arts for funding through the International Graduate School "Materials Science of Complex Interfaces" (CompInt). This work was financially supported by DFG in the priority program for nano and microfluids SPP1164 (Grant MU1487/2). S.V.R. acknowledges the European Synchrotron Radiation Facility for provision of synchrotron radiation facilities. We thank Lionel Lardiere for assistance in using beamline ID13.

References and Notes

(1) Romero, D. B.; Schaer, M.; Staehli, J. L.; Zuppiroli, L.; Widawski, G.; Rawiso, M.; Francois, B. *Solid State Commun.* **1995**, *95*, 185.
(2) Heeger, A. J. *Curr. Appl. Phys.* **2001**, *1*, 247.
(3) Coakley, K. M.; McGehee, M. D. *Appl. Phys. Lett.* **2003**, *83*, 3380.
(4) Tzanetos, N. P.; Dracopoulos, V.; Kallitsis, J. K.; Deimede, V. A. *Langmuir* **2005**, *21*, 9339.
(5) Woodson, M.; Liu, J. *J. Am. Chem. Soc.* **2006**, *128*, 3760.
(6) Yu, G.; Gao, J.; Hummelen, J. C.; Wudl, F.; Heeger, A. J. *Science* **1995**, *270*, 1789.
(7) Greenham, N. C.; Moratti, S. C.; Bradley, D. D. C.; Friend, R. H.; Holmes, A. B. *Nature (London)* **1993**, *365*, 628.
(8) Castro, F. A.; Benmansour, H. C.; Graeff, C. F. O.; Nuesch, F.; Tutis, E.; Hany, R. *Chem. Mater.* **2006**, *18*, 5504.
(9) Li, K.; Guo, H.; Liang, Z. Q.; Thiyagarajan, P.; Wang, Q. *J. Polym. Sci., Part A: Polym. Chem.* **2005**, *43*, 6007.
(10) Loos, K.; Boker, A.; Zettl, H.; Zhang, A. F.; Krausch, G.; Muller, A. H. E. *Macromolecules* **2005**, *38*, 873.
(11) Wang, H. B.; Wang, H. H.; Urban, V. S.; Littrell, K. C.; Thiyagarajan, P.; Yu, L. P. *J. Am. Chem. Soc.* **2000**, *122*, 6855.
(12) Leclere, P.; Hennebicq, E.; Calderone, A.; Brocorens, P.; Grimsdale, A. C.; Mullen, K.; Bredas, J. L.; Lazzaroni, R. *Prog. Polym. Sci.* **2003**, *28*, 55.
(13) Hempenius, M. A.; Langeveld-Voss, B. M. W.; van Haare, J.; Janssen, R. A. J.; Sheiko, S. S.; Spatz, J. P.; Moller, M.; Meijer, E. W. *J. Am. Chem. Soc.* **1998**, *120*, 2798.
(14) Bates, F. M.; Fredrickson, G., H. *Annu. Rev. Phys. Chem.* **1990**, *41*, 525.
(15) Hamley, I. W. *The Physics of Block Copolymers*; Oxford University Press: New York, 1998.
(16) Russell, T. P. *Science* **2002**, *297*, 964.
(17) Kadota, S.; Aoki, K.; Nagano, S.; Seki, T. *J. Am. Chem. Soc.* **2005**, *127*, 8266.
(18) Ludwigs, S.; Schmidt, K.; Krausch, G. *Macromolecules* **2005**, *38*, 2376.
(19) Spontak, R. J.; Shankar, R.; Bowman, M. K.; Krishnan, A. S.; Hamersky, M. W.; Samseth, J.; Bockstaller, M. R.; Rasmussen, K. O. *Nano Lett.* **2006**, *6*, 2115.

(20) Fasolka, M. J.; Harris, D. J.; Mayes, A. M.; Yoon, M.; Mochrie, S. G. J. *Phys. Rev. Lett.* **1997**, *79*, 3018.
(21) Smith, A. P.; Douglas, J. F.; J. Carson Meredith, J.; Amis, E. J.; Karim, A. *Phys. Rev. Lett.* **2001**, *87*, 015503.
(22) Horvat, K. A.; Lyakhova, K. S.; Krausch, G.; Sevink, G. J. A.; Zvelindovsky, A. V.; Magerle, R. *Phys. Rev. Lett.* **2002**, *89*, 035501.
(23) Ludwigs, S.; Schmidt, K.; Stafford, C. M.; Amis, E. J.; Fasolka, M. J.; Karim, A.; Magerle, R.; Krausch, G. *Macromolecules* **2005**, *38*, 1850.
(24) Lee, M.; Cho, B.-K.; Zin, W.-C. *Chem. Rev.* **2001**, *101*, 3869.
(25) Olsen, B. D.; Segalman, R. *Macromolecules* **2006**, *39*, 7078.
(26) Chen, L. J. T.; Thomas, E. L.; Ober, C. K.; Mao, G. P. *Science* **1996**, *273*, 343.
(27) Chen, X. L.; Jenekhe, S. A. *Macromolecules* **2000**, *33*, 4610.
(28) Cornelissen, J. J. L. M.; Fischer, M.; Sommerdijk, N. A. J. M.; Nolte, R. J. M. *Science* **1998**, *280*, 1427.
(29) Tenneti, K. K.; Chen, X. F.; Li, C. Y.; Tu, Y. F.; Wan, X. H.; Zhou, Q. F.; Sics, I.; Hsiao, B. S. *J. Am. Chem. Soc.* **2005**, *127*, 15481.
(30) Jenekhe, S. A.; Chen, X. L. *Science* **1998**, *279*, 1903.
(31) Matsen, M. W.; Barrett, C. *J. Chem. Phys.* **1998**, *109*, 4108.
(32) Halperin, A. *Europhys. Lett.* **1989**, *10*, 549.
(33) Cimrova, V.; Remmers, M.; Neher, D.; Wegner, G. *Adv. Mater.* **1996**, *8*, 146.
(34) Tolan, M. *X-Ray Scattering from Soft-Matter Thin Films*; Springer: Berlin, 1999.
(35) Salditt, T.; Metzger, T. H.; Peisl, J.; Jiang, X. *J. Phys. III* **1994**, *4*, 1573.
(36) Rauscher, M.; Paniago, R.; Metzger, H.; Kovats, Z.; Domke, J.; Pfannes, H. D.; Schulze, J.; Eisele, I. *J. Appl. Phys.* **1999**, *86*, 6763.
(37) Müller-Buschbaum, P. *Anal. Bioanal. Chem.* **2003**, *376*, 3.
(38) Müller-Buschbaum, P.; Stamm, M. *Physica B* **1998**, *248*, 229.
(39) Müller-Buschbaum, P.; Gutmann, J. S.; Stamm, M. *Phys. Chem. Chem. Phys.* **1999**, *1*, 3857.
(40) Müller-Buschbaum, P.; Bauer, E.; Maurer, E.; Schlögl, K.; Roth, S. V.; Gehrke, R. *Appl. Phys. Lett.* **2006**, *7*, 1773.
(41) Müller-Buschbaum, P.; Roth, S. V.; Burghammer, M.; Diethert, A.; Panagiotou, P.; Riekel, C. *Europhys. Lett.* **2006**, *88*, 083114.
(42) Roth, S. V.; Walter, H.; Burghammer, M.; Riekel, C.; Lengeler, B.; Schroer, C.; Kuhlmann, M.; Walther, T.; Sehrbrock, A.; Domnick, R.; Müller-Buschbaum, P. *Appl. Phys. Lett.* **2007**, *91*, 091915.
(43) Roth, S. V.; Autenrieth, T.; Grübel, G.; Riekel, C.; Burghammer, M.; Hengstler, R.; Schulz, L.; Müller-Buschbaum, P. *Appl. Phys. Lett.* **2007**, *88*, 021910.
(44) Roth, S. V.; Burghammer, M.; Riekel, C.; Müller-Buschbaum, P.; Diethert, A.; Panagiotou, P. *Appl. Phys. Lett.* **2003**, *82*, 1935.
(45) Müller-Buschbaum, P.; Gebhardt, R.; Maurer, E.; Bauer, E.; Gehrke, R.; Doster, W. *Biomacromolecules* **2006**, *7*, 1773.
(46) Müller-Buschbaum, P.; Gebhardt, R.; Roth, S. V.; Metwalli, E.; Doster, W. *Biophys. J.* **2007**, *93*, 960.
(47) Tuzar, Z.; Kratochvil, P. *Adv. Colloid Interface Sci.* **1976**, *6*, 201.
(48) Lazzaron, R.; Lecltrea, Ph.; Couturiaux, A.; Parentea, V.; Francois, B.; Bredas, J. L. *Synth. Met.* **1999**, *102*, 1279.
(49) Russell, T. P.; Kim, S. H.; Misner, M. J.; Xu, T. *Adv. Mater.* **2004**, *16*, 226.